Geometry and stiffness optimization for switches and crossings, and simulation of material degradation

D Nicklisch, E Kassa, J Nielsen, M Ekh and S Iwnicki

Proceedings of the Institution of Mechanical Engineers, Part F: Journal of Rail and Rapid Transit 2010 224: 279
DOI: 10.1243/09544097JRRT348

Geometry and stiffness optimization for switches and crossings, and simulation of material degradation

D Nicklisch[1], **E Kassa**[2*], **J Nielsen**[3], **M Ekh**[3], and **S Iwnicki**[2]
[1]DB Systemtechnik, Deutsche Bahn AG, Munich, Germany
[2]Department of Engineering and Technology, Rail Technology Unit, Manchester Metropolitan University, Manchester, UK
[3]CHARMEC/Department of Applied Mechanics, Chalmers University of Technology, Gothenburg, Sweden

The manuscript was received on 18 November 2009 and was accepted after revision for publication on 26 March 2010.

DOI: 10.1243/09544097JRRT348

Abstract: A methodology for simulating wear, rolling contact fatigue, and plastic deformation for a mixed traffic situation in switches and crossings (S&C) has been developed. The methodology includes simulation of dynamic vehicle–track interaction considering stochastic variations in input data, simulation of wheel–rail contacts accounting for non-linear material properties and plasticity, and simulation of wear and plastic deformation in the rail during the life of the S&C component. To find means of improving the switch panel design, the geometry of a designed track gauge variation in the switch panel has been represented in a parametric way. For traffic in the facing and trailing moves of the through route, an optimum solution was identified and then validated by evaluating a wide set of simulation cases (using different wheel profiles). The optimum design includes a 12 mm maximum gauge widening. Several crossing geometries were investigated to find an optimal geometric design for the crossing nose and wing rails. The MaKüDe design showed the best performance for moderately worn wheel profiles in both running directions (facing and trailing moves). In connection with reduced support stiffness (e.g. elastic rail pads), this crossing design is predicted to lead to a significant reduction of impact loads and consequently provide a high potential of life-cycle cost reduction.

Keywords: switches and crossings, track gauge, track stiffness, wear, plastic deformation

1 INTRODUCTION

Switches and crossings (S&C or turnouts) are comprised of a switch panel and a crossing panel connected by a closure panel. The different components of an S&C are illustrated in Fig. 1. They are important elements in a railway network, as they provide flexibility to traffic operation. However, in a railway system, the maintenance cost for S&C is very high in comparison with plain line. For example, the largest contribution of reported track faults is associated with S&C.

Wear and accumulated plastic deformation are common damage mechanisms in S&C components. Examples of damage, as illustrated in Fig. 2, are as follows:

(a) a part of the switch blade has been detached;
(b) wear and plastic deformation have developed on the crossing noses and on the wing rail.

Rolling contact fatigue (RCF) is another type of damage mechanism that leads to surface cracks on the rails. To predict the overall degradation of S&C components, it is necessary to consider all three damage mechanisms: plastic deformation, RCF, and wear. The maintenance effort related to S&C can be reduced by using more durable materials and optimized turnout design. These require detailed understanding of the dynamics in S&C, the resulting forces, and their effect on the degradation modes.

The dynamics of a vehicle in S&C is far more complex than on ordinary tangent or curved tracks. The geometrical design, dictated by the function of an S&C, leads to additional disturbances compared to the normal response of a vehicle on plain line track. The largest disturbances occur in the switch panel when the wheels are transferred from stock rail to the switch

*Corresponding author: *Department of Engineering and Technology, Rail Technology Unit, Manchester Metropolitan University, John Dalton Building, Chester Street, Manchester M1 5GD, UK.*
email: elias.kassa@gmail.com

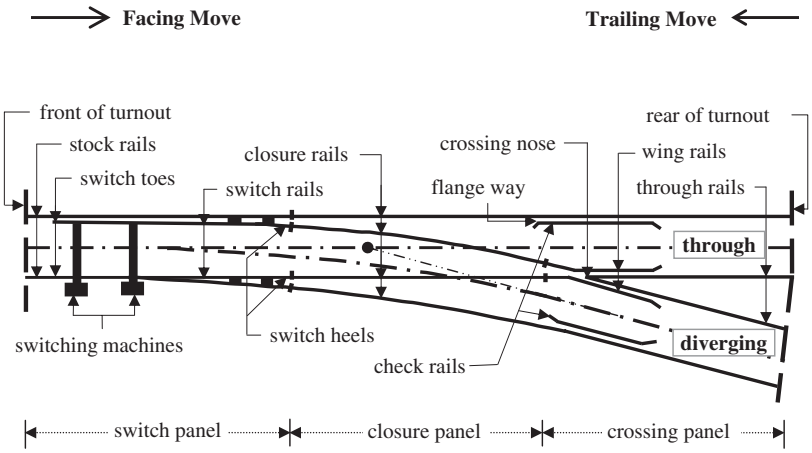

Fig. 1 Components of a turnout

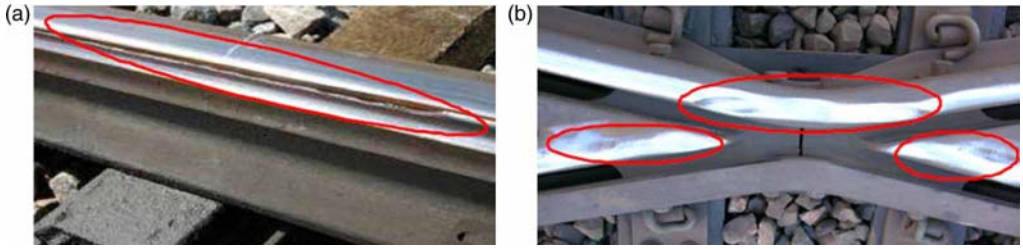

Fig. 2 Examples of damage on switch components: (a) part of the switch rail is detached and (b) damage due to plastic deformation and wear on crossing noses and wing rail

rail and in the crossing panel when the wheels pass the gap between wing rail and nose rail.

A railway vehicle running in the switch panel often experiences significant lateral displacements, sometimes leading to wheel flange contact. This leads to increased wheel and rail wear and sometimes RCF problems on the rails. Severe impact loads may also be generated when wheels transfer between wing rail and crossing nose in the crossing panel. The magnitude of the impact force is influenced by several parameters, such as the design and manufacturing tolerances of the crossing, service condition of wheel, wing rail and crossing nose, track stiffness (voided sleepers, use of under sleeper pads, etc.), axle load, vehicle speed, and lateral position of the wheel when approaching the crossing nose. Simulation tools have been developed to calculate wheel–rail contact forces, wheel–rail contact stresses, wear index, and an RCF index at key components in the S&C [**1**–**3**].

This work was carried out as part of the EC Framework 6 project, INNOTRACK, under a subproject dealing with S&C. The objective of part of the work is the development of innovative S&C designs that allow for increased axle loads and speeds and that lead to a decreased need for maintenance. This paper presents a methodology for optimizing the track geometry and support stiffness in the switch panel, for optimizing the transition geometry and support stiffness of the superstructure at the crossing panel, and for predicting deterioration of S&C components due to wear and plastic deformation.

2 OPTIMIZATION IN THE SWITCH PANEL

In S&C, when a vehicle is running in the diverging route, large lateral wheelset displacements are developed, leading to severe flange contact with the curved switch rail. This is mainly due to the abrupt change in track curvature and the large cant deficiency. It has also been observed that vehicles running on the through route in the switch panel often experience significant lateral wheelset displacements, sometimes leading to flange contact with the straight switch rail. These flange contacts result in an increase in wear of the switch rails and on some occasions in RCF problems on the rails, requiring increased inspection and maintenance and leading to reduced life of the components.

The rail cross-section varies continuously along the switch panel. At the switch panel entry, there is only one full rail cross-section on each side of the track. Additional rails are then introduced on each side, with their cross-sections varying from a thin section at the switch toe to a full-sized rail cross-section at the switch heel. These additional rails lead to a continuous change in track stiffness, which has been shown by track receptance measurements at several locations in an S&C (see reference [**4**]).

The vertical track stiffness in the switch panel can be optimized, possibly by adjusting the rail pad stiffness or by use of under sleeper pads. In this way, the abrupt changes in track stiffness, due to the appearance of two rails and changes in rail cross-section, could be reduced and wheel–rail contact forces minimized. In addition, it is possible to reduce the tangential contact forces and hence wear of the switch rail in the switch panel by optimizing the track gauge at the switch panel entry by applying dynamic gauge widening.

Simulations of a vehicle passing an S&C have been performed using the multi-body dynamics code SIMPACK. A freight vehicle model, with a car body and two Y25 bogies, is used. In the simulations, the vehicle model is allowed to run on a length of tangent track before entering the turnout, which has constant curvature geometry. The turnout geometry is a standard S&C design (UIC60-760-1:15) with curve radius 760 m and turnout angle 1:15.

The track model is based on a moving mass–spring–damper system with seven degrees of freedom coupled to each wheelset [**1**]. Two masses representing the rail masses are connected with the track mass by two spring–damper pairs k_p to represent the combined rail and rail pad stiffness. The remaining flexibility (the structure underneath the rail pad) is represented by a spring–damper element k_b connecting the track mass with the ground. The track model parameter values are varying along the switch panel. This is done by varying the values of the rigid masses and the spring–damper elements within the model. Measured vertical track receptances, with single-point excitation applied on the rail head of the switch and stock rails, have been used to characterize the track.

2.1 Optimization of track gauge

Simulations of a train passing a turnout in facing and trailing moves have been performed to understand the underlying phenomenon and to devise a strategy for the gauge optimization process. When a train traverses a switch panel, the wheelset tries to follow the path dictated by the stock rails of the switch. For the through route, the wheel load transfers from the curved stock rail fully to the straight switch rail a few metres after the stock rail enters the curved path. An artificial increase in the gauge is taking place on the side of the switch as the wheel follows the curved stock rail, and therefore a rolling radius difference is generated between the two wheels. This causes a yaw moment and subsequent lateral force resulting in a movement of the whole wheelset towards the switch rail. When the load is finally transferred to the straight switch rail, a sudden reduction in gauge takes place on one side, which forces the wheelset towards the other side of the track. The same phenomenon can be depicted for the diverging route.

To balance the artificial gauge increase generated due to the contact point trajectories in the switch panel, two possible dynamic gauge-widening geometries are proposed, one for each route [**1**]. In this paper, track gauge optimization for the through route is only discussed. Dynamic gauge widening applies a continuous variation of the gauge by moving the straight stock rail laterally at the switch entry, which results in a gauge increase. The optimization process has been carried out using only one type of vehicle model, a freight vehicle model with Y25 bogies, and a typical wheel profile in the simulations. The vehicle was simulated running in the facing moves, and the performance of the optimized geometry is assessed later in the trailing moves. The optimized geometry was then evaluated with several load cases consisting of 18 different measured wheel profiles in terms of wear index, normal contact forces, RCF index, and contact point position on the rail.

The geometry of the gauge variation is parameterized by three variables. It consists of four circular curves, see Fig. 3(a). The three variables representing the parameterized gauge optimization model are L_1, R_{Out}, and L_{Total}. At the very first zone of the switch, the diverging rail becomes curved with given radius R_C (corresponding to the curvature of the diverging route). In this zone, the same radius R_C is used for the stock rail. Thus, the track centre-line is kept unchanged, and the wheelset would be expected to suffer no lateral excitation. The variable L_1 represents the length for which the sign of the curvature is

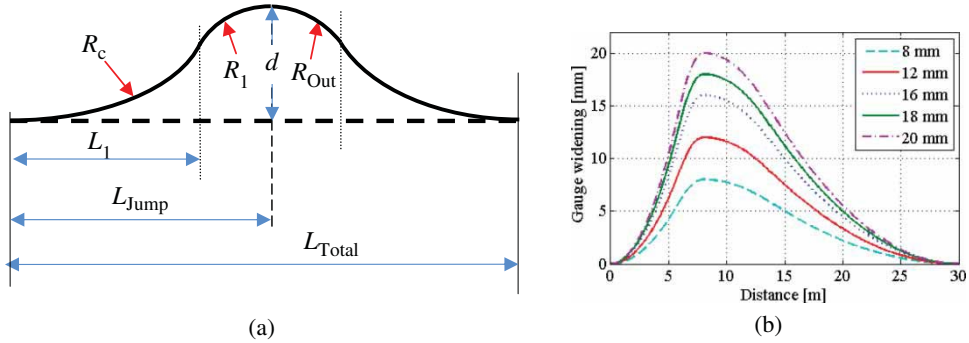

Fig. 3 (a) Gauge optimization parameters and (b) levels of dynamic gauge widening

changed. For the nominal case, the wheel load transfers fully from the stock rail to the switch rail at the contact point jump location, L_{Jump}. The second variable R_{Out} represents the curvature of the stock rail after the jump point has passed. The third variable is L_{Total}, and this defines the total length of the dynamic gauge variation from the beginning of the turnout. It effectively controls how rapidly the gauge returns to normal at the final zone of the gauge variation. The influence of the last two variables is not significant when simulating the facing move, as their effect comes after the contact point jump. The critical location that needs gauge modification is the area of load transfer in the switch panel. Therefore, the two variables R_{out} and L_{Total} can be predefined to have large values that will not bring any interference on the dynamics when the wheelset runs in the crossing panel. This results in a single variable, L_1, left to be assessed. For a given turnout geometry with radius R_{C} and known contact jump point (L_{Jump}), the variable L_1 is directly related to the maximum amplitude of the gauge increase d.

Finding an optimal design for the dynamic gauge widening is performed by varying the values of the parameter d so that wheel–rail contact forces and wear can be minimized. Five different levels of maximum gauge increase are evaluated: $d = \{8, 12, 16, 18 \text{ and } 20\,\text{mm}\}$, see Fig. 3(b). The geometry of the turnout studied has $R_{\text{C}} = 760\,\text{m}$. The contact point jump location for the nominal case was $L_{\text{Jump}} \approx 7.5\,\text{m}$. The total length of the dynamic gauge variation was taken $L_{\text{Total}} = 25\,\text{m}$ and $R_{\text{out}} = 2280\,\text{m}$ (three times R_{C}).

Several outputs were assessed to determine the optimal dynamic gauge-widening geometry, here represented by the amplitude of the gauge widening, d. The best geometry that proves to give a reduced deviation of the wheelset lateral position from the central position, contact point locations away from the wheel flange, reduction in wear indices, and reduction in normal contact forces is taken to be the optimal design.

Figure 4 shows the influence of different gauge-widening amplitudes on the normal wheel–rail contact force. The results are compared with the nominal design. The smallest (8 mm) and the largest (20 mm) amplitude designs result in high transients between 8 and 8.5 m from switch entry. This happens when the load is fully transferred from a two-point contact (the first contact point is the contact on the stock rail, whereas the second contact point is the contact on the switch rail) to a single-point contact on the switch rail. For the other studied gauge-widening amplitudes, there is no significant change in the normal contact force before or after the contact jump. However, the appearance of the second contact point, contact on the switch rail, is delayed by 30–40 cm.

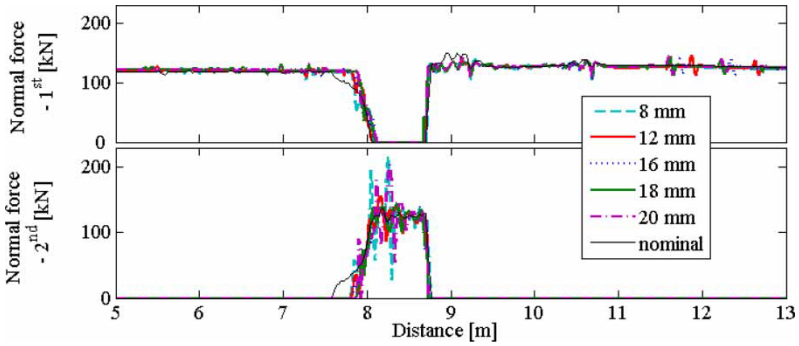

Fig. 4 Wheel-rail normal contact force in the switch panel for different gauge-widening amplitudes. First contact point (top) and second contact point (bottom). Vehicle in facing move of through route

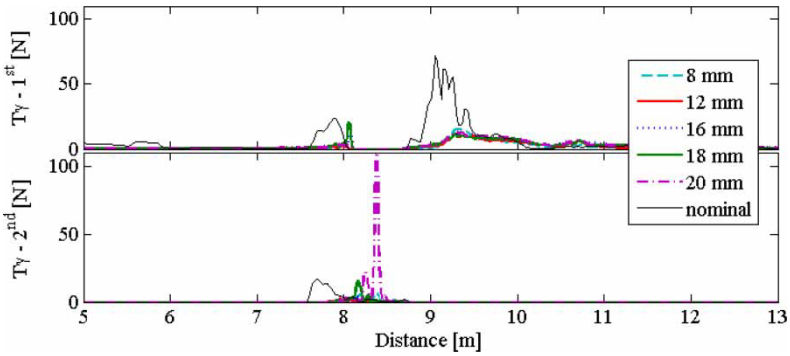

Fig. 5 Wear index $T\gamma$ in the switch panel for different gauge-widening amplitudes. First contact point (top) and second contact point (bottom). Vehicle in facing move of through route

For the two contact points, the calculated wear indices along the switch panel for all levels of gauge-widening amplitudes are shown in Fig. 5. Wear index ($T\gamma$) is defined as

$$T\gamma = |T_x\gamma_x| + |T_y\gamma_y| \tag{1}$$

where T_x, γ_x, T_y, and γ_y are creep forces and creepages in lateral and longitudinal directions, respectively. It is observed that the application of a dynamic gauge widening leads to a reduction in wear index along the switch panel and that the maximum value of the wear index is reduced considerably for gauge-widening amplitudes 8–16 mm. However, the 20 mm gauge amplitude leads to an increase in wear index, and the reduction using the 18 mm gauge amplitude design is not significant compared to the other designs.

The two designs of dynamic gauge widening (12 and 16 mm), which were proved to be optimal in the facing move, were subsequently evaluated in the trailing move with respect to wear index. Figure 6 shows the predicted wear indices in the switch panel for the trailing move, with distance measured from the beginning of the S&C. For the 16 mm gauge widening, contrary to the facing move, the wear index is slightly increased both in the first and in the second contacts. In addition, the location of the maximum wear index on the switch rail has shifted towards the switch toe, where the thickness of the switch rail is smaller. As in the case of the facing move, the 12 mm gauge-widening amplitude leads to a significant improvement in reducing the wear index. Therefore, the design corresponding to the 12 mm maximum gauge widening is the optimal design for both the facing and the trailing moves.

To further evaluate the optimum design, simulations were carried out using 18 measured wheel profiles. The performance of the optimal design was also assessed with respect to RCF. The engineering model for prediction of RCF impact developed by Ekberg *et al.* [**5**] was used assuming that the energy input represented by the fatigue parameter affects both rail and wheel equally. The surface-initiated RCF index FI_{surf} is expressed as

$$FI_{\text{surf}} = \frac{\sqrt{T_x^2 + T_y^2}}{F_{\text{n}}} - \frac{2\pi abk}{3F_{\text{n}}} \tag{2}$$

where F_{n} is the normal contact force, T_x and T_y are the creep forces in the longitudinal and lateral directions, a and b are the semiaxes of the Hertzian contact patch, and k is the yield limit in pure shear (here taken as 300 MPa). Surface-initiated RCF is predicted

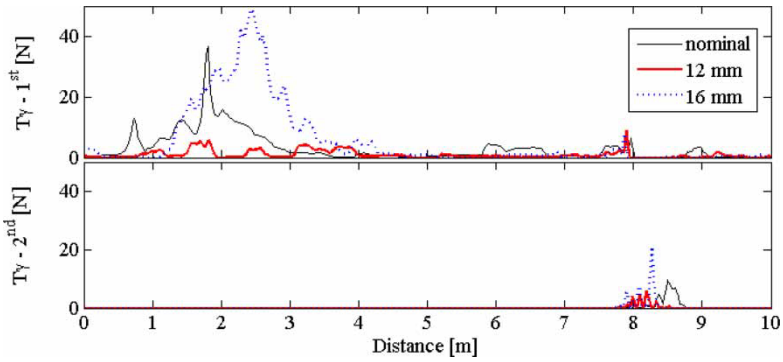

Fig. 6 Wear indices $T\gamma$ in the switch panel. First contact point (top) and second contact point (bottom). Vehicle in trailing move of through route

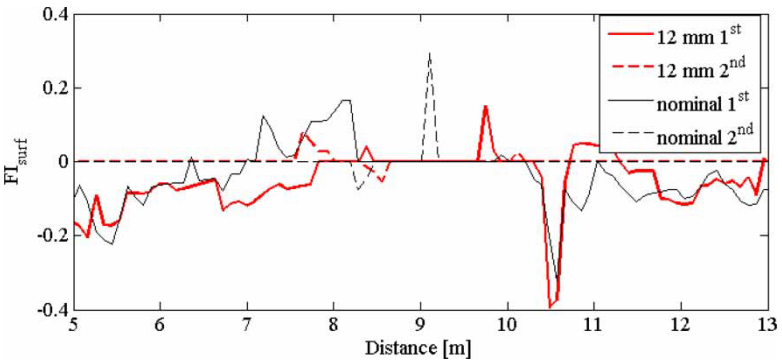

Fig. 7 Maximum rolling contact fatigue index FI_{surf} along the switch panel for the nominal and optimized geometry. Vehicle in facing move of through route

to occur if $FI_{surf} > 0$. Based on simulations with 18 different wheel profiles, the maximum FI_{surf} is shown in Fig. 7. The limit for RCF prediction is exceeded at more locations for the nominal S&C design compared to the gauge-optimized geometry. Thus, with the adopted geometrical representation of gauge widening, the switch panel design corresponding to the 12 mm maximum gauge widening is the optimal design for the through route, both for the facing and for the trailing moves.

2.2 Optimization of track stiffness

The vertical track receptance was measured at several locations along a similar turnout at Härad in Sweden [**4**], and the values measured at three locations in the switch panel (location 1 = 4.5 m, location 2 = 9.1 m, and location 3 = 21.85 m from the front of the S&C) were used to determine input data for a track model. The track model vertical receptance is in good agreement with measured track receptance in the frequency range up to 400 Hz [**1**]. It was observed that the rail (and rail pad) stiffness at the second measurement location (9.1 m) was increased by 40 per cent compared to the corresponding stiffness at measurement point 1 (4.5 m). The stiffness increased by 70 per cent at the third measurement location (21.85 m) compared to the first point.

Two alternative stiffness variation models are developed to smooth out this large change in track stiffness along the switch panel. Here, the maximum variations of the track stiffness at the three locations are limited to ±30 per cent. The ±30 per cent change is expected to be gained by adjusting the rail pad stiffness. The aim is mainly to investigate the influence of the rail pad stiffness variation in the global track stiffness along the switch and, hence, on the wheel–rail contact forces.

Compared to the track model that was tuned based on track receptance measurements, the value of the rail/rail pad stiffness k_p in the first stiffness optimization model (k_p_v1) was increased by 30 per cent at location 1 and reduced by 15 per cent at location 3, keeping the value at location 2 unchanged. This gives rise to k_p-values along the switch panel: 416.0, 448.0, and 462.4 MN/m at locations 1, 2, and 3, respectively. The stiffness values in the second model (k_p_v2) lead to a further reduction of the stiffness increase between locations 1 and 3, down to about 8 per cent. This is obtained by increasing the value of k_p at location 1 by 28 per cent from the measured value and reducing it by 6 per cent and 19 per cent at locations 2 and 3, respectively. This gives values of k_p at the three locations of 409.6, 441.6, and 454.4 MN/m. The stiffness variation is now relatively constant throughout the switch panel. This can be achieved by placing stiffer rail pads starting from some distance before the front of the turnout and softer rail pads close to the switch heel.

The optimization was performed for one load case. The vehicle model was simulated in the facing move of the through route and with the three different track stiffness arrangements: nominal (k_p_nom), variation 1 (k_p_v1), and variation 2 (k_p_v2). Figure 8 shows the wear indices for the three stiffness variation cases. The maximum wear index for the second contact point (at about 8.2 m) for the nominal case is 10 N. A slight reduction is obtained, 9.3 and 7.5 N, when using the k_p_v1 and k_p_v2 model arrangements, respectively.

Together with the k_p-variation, an optimization of the spring–damper element stiffness for the sleeper/ballast structure k_b has also been considered. The k_b stiffness value was increased by 20 per cent at location 1, reduced by 10 per cent at location 2, and reduced by 20 per cent at location 3, corresponding to 39, 41, and 46.8 MN/m, respectively.

Wear indices along the switch panel for different combinations of variations in k_p and k_b are shown in Fig. 9. Maintaining the nominal k_p-values, while varying k_b, reduces the wear index at the second contact point by almost 50 per cent, from 10 to 5.3 N. A relatively large reduction in the wear index is obtained when optimized k_p and k_b stiffness values are used in combination. The reduction is seen at both the first and the second contact points. At the first contact point, the maximum wear index (at 10.7 m) is

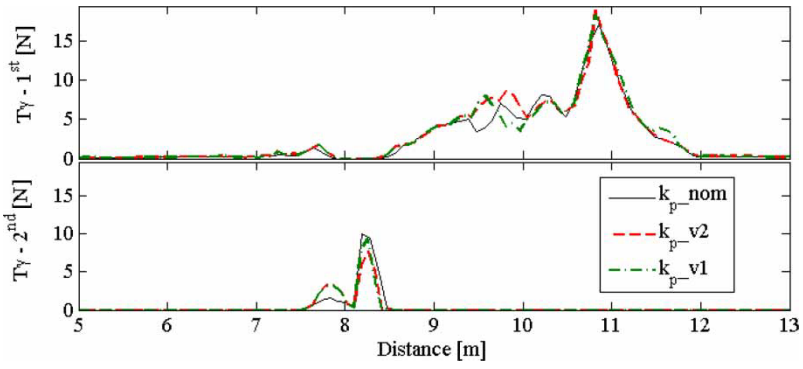

Fig. 8 Wear indices $T\gamma$ for three variations of k_p. First contact point (top) and second contact point (bottom). Vehicle in facing move of through route

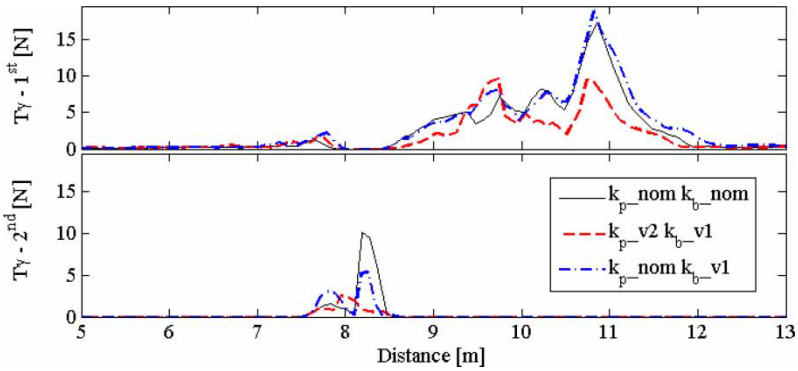

Fig. 9 Wear indices $T\gamma$ with combinations of variations in k_p and k_b. First contact point (top) and second contact point (bottom). Vehicle in facing move of through route

reduced by 50 per cent from 18.9 to 9.5 N. The maximum wear index at the second contact is reduced by more than the sum of the individual reduction to only 2.2 N, i.e. an 80 per cent reduction is obtained. The conclusion is that the optimum arrangement corresponds to a minimum variation in support stiffness along the switch.

3 OPTIMIZATION IN THE CROSSING PANEL

Severe impact loads may be generated when wheels transfer between wing rail and crossing nose in the crossing panel. These large contact forces lead to a deterioration of the crossing nose by different damage mechanisms. Thus, in order to minimize the material degradation induced by wheels passing the frog (crossing nose and wing rails), the transition geometry and support stiffness of the superstructure are optimized.

The influence of different system parameters, and operational and service conditions on impact loads generated on a German standard crossing EH 60-500-1:12 were evaluated to identify the optimum design. This was studied by varying a number of parameters, such as static wheel load, train speed, wheel profile, initial lateral wheel position at crossing entry, track stiffness (including unsupported sleepers), and running direction (facing and trailing move). Because of the higher speed and consequently higher impact loads compared to the diverging route, only the through route of the turnout was considered.

The simulations were performed with complete three-dimensional (3D) vehicle models of a Loco BR 101 and of an ICE-T coach (BR 411), representing two different wheel loads (Loco BR 101 : $Q_0 = 107$ kN, ICE-T coach: $Q_0 = 67$ kN). Three different wear states of the wheel profiles were used: nominal S1002, medium worn, and hollow worn. The track was represented by a finite element model (FEM) consisting of elastic rails and elastically supported elastic sleepers, which are arranged according to the layout of the turnout. The changing dynamic properties of the track within the turnout are represented by position-dependent parameters such as rail cross-section and sleeper mass. The values were chosen according to a common ballasted track turnout at Deutsche Bahn (DB). For more detailed discussion of the track model, see reference [**2**]. The investigation was based on the assumption that the maximum normal wheel–rail contact force is representative for the material degradation of the frog.

3.1 Optimization of crossing nose transition geometry

Two general approaches have been studied for the optimization of transition geometry of rigid (non-movable) crossings. The first one has the target to prevent the wheel from making contact with the crossing nose at a section too weak to withstand the impact loads. The second approach aims at smoothing the vertical wheel movement during the transition between wing rail and crossing nose to reduce the impact loads. On the basis of these approaches, several alternative frog geometries have been investigated:

(a) reduction of the flange-way width between crossing nose and wing rail within the allowed tolerances, in order to delay the transition area to a thicker cross-section of the crossing nose;
(b) profiling of the frog by following a kinked ramp to decrease the gradient of the vertical wheel movement after transition to the crossing nose (optimization for facing move);
(c) super-elevation of the wing rail and profiling with a negative wheel shape to reduce the vertical wheel movement (MaKüDe, design developed by DB Systemtechnik), see Fig. 10(a).

Figure 10(b) shows examples of the vertical wheel movement for an S1002 wheel profile for the three proposed designs compared to the nominal frog geometry. The vertical wheel movement for a short version of the kinked ramp design, which has the same effect

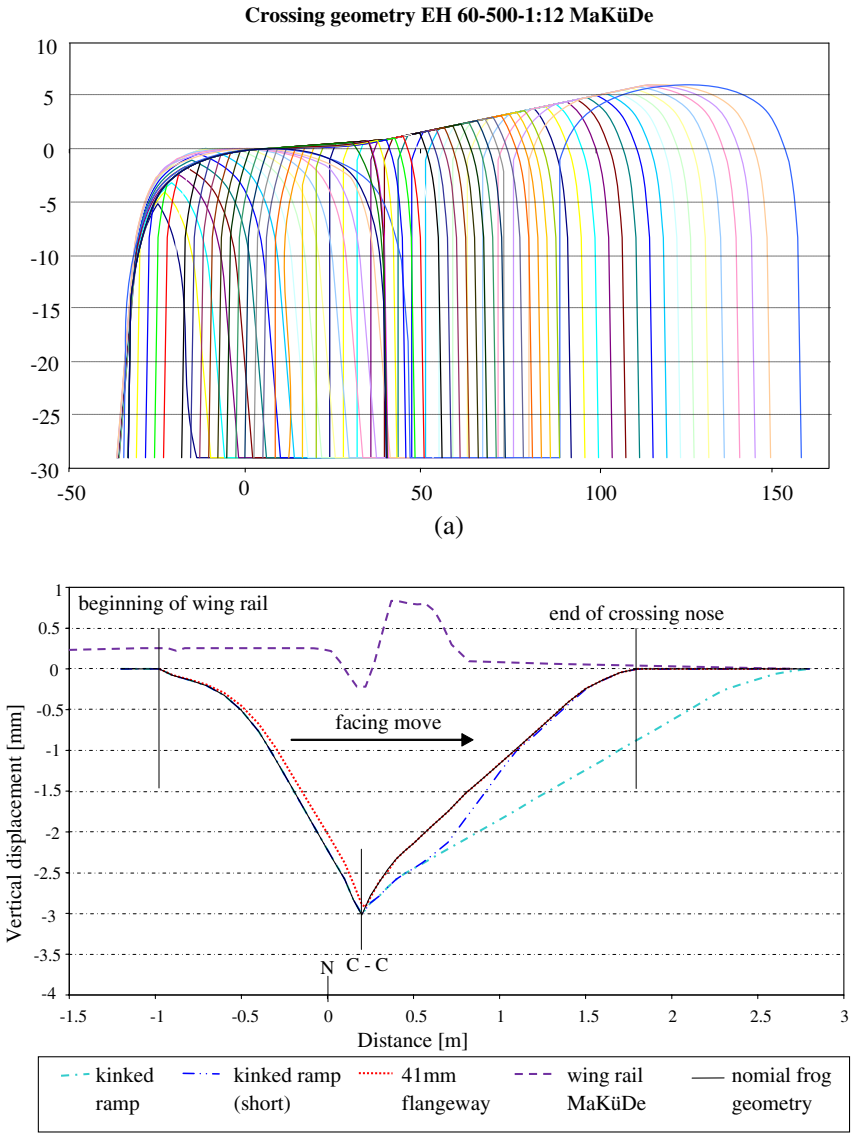

Fig. 10 (a) Cross-sections of MaKüDe design (frog and right wing rail) and (b) comparison of vertical wheel movement for different transition designs (wheel profile S1002). Point N indicates the tip of the crossing nose (Distance=0 m), C–C is the theoretical point of wheel transition

on the impact loads in the transition area as the longer version, is also shown in Fig. 10(b).

Initiated by the known problem of wing rail damage caused by hollow-worn wheels passing in the trailing move, another modification of the nominal crossing design was investigated. In trailing move, the outer section of a hollow-worn wheel arrives too deep and hits the gauge corner of the wing rail. To avoid this, a small chamfer was added on the wing rail flange to reduce the contact angle when the wheel is transferred to the wing rail. This effect is illustrated in Fig. 11.

Maximum normal contact forces $F_{\mathrm{n,max}}$ and maximum von Mises equivalent stresses $\sigma_{\mathrm{e,max}}$ for the alternative crossing designs are presented in Fig. 12. For the theoretical S1002 wheel profile, the biggest force reduction (up to 50 kN) can be reached with the kinked ramp design, whereas the MaKüDe design leads to even higher normal contact forces than the nominal design. This is caused by the steep gradient of the wheel movement after transition to the crossing nose (see Fig. 10(b)). For worn wheels, the effect is inverted. Here, the MaKüDe design provides by far the lowest normal contact forces. For the medium-worn wheel profile, the MaKüDe design leads to a peak force reduction of nearly 50 per cent.

Looking at the calculated von Mises equivalent stresses, trends different from that for the normal contact forces can be observed. The reason is that the maximum normal contact force occurs at a location different from the maximum equivalent stress. At

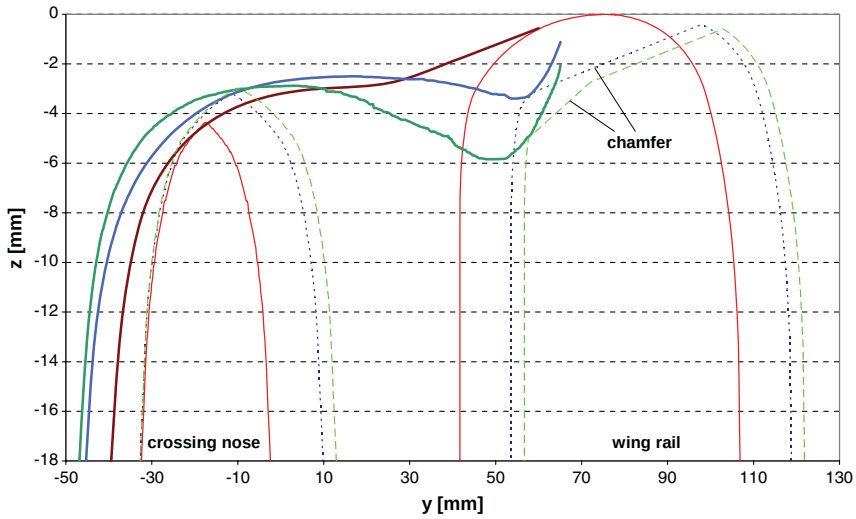

Fig. 11 Contact situations at the point of wheel transition for new and hollow-worn wheel profiles on a chamfered wing rail. The severely worn wheel (green thick line) will be transferred at the cross-section with a deep chamfer (green dashed), the moderately hollow-worn wheel (blue thick line) at the cross-section with a shallow chamfer (blue dotted), and the new wheel (brown thick line) at the nominal transition point represented by the red cross-section

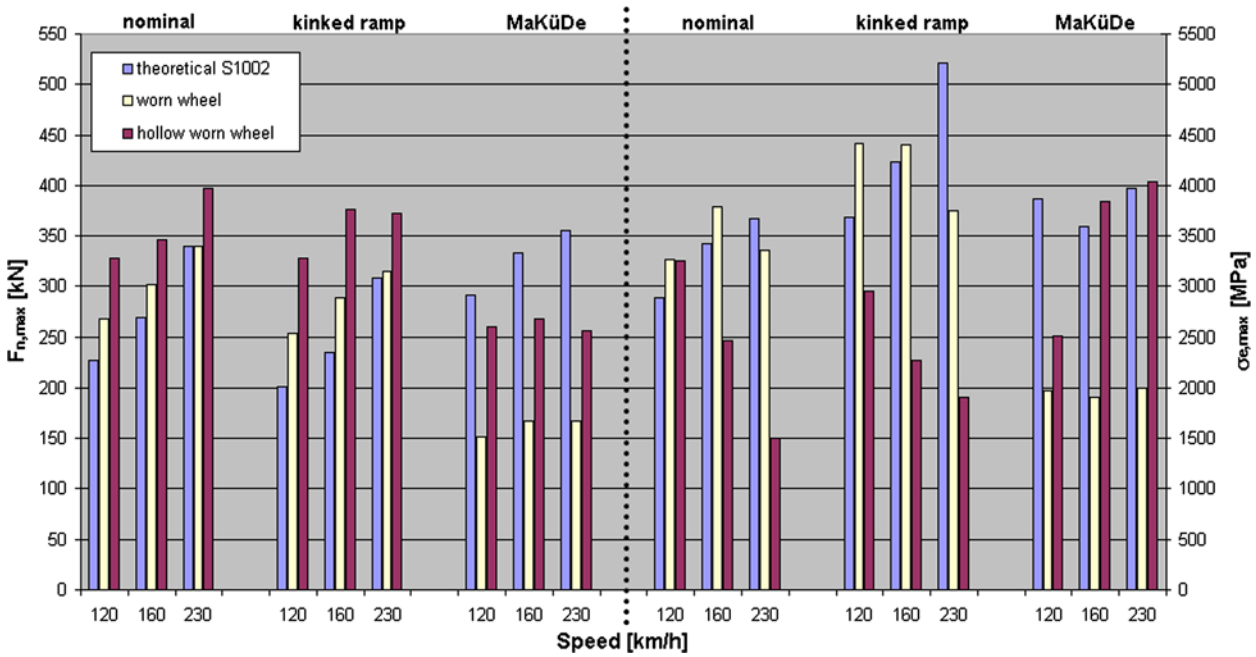

Fig. 12 Influence of transition geometry, wheel profile, and train speed on maximum normal contact force and equivalent stress. Loco BR 101 ($Q_0 = 107$ kN), 500 kN/mm, facing move

some locations, relatively low normal contact forces may cause very high contact stresses and vice versa, due to the differences of the rail profile geometry and consequently contact patch size. Only for the MaKüDe design passed by worn wheels, both an evaluation in terms of maximum normal contact force and an equivalent contact stress lead to the same conclusion. In this case, the MaKüDe design provides the best performance with respect to both criteria.

3.2 Optimization of track stiffness

In order to obtain some information on the distribution of the impact loads on crossings, the influence

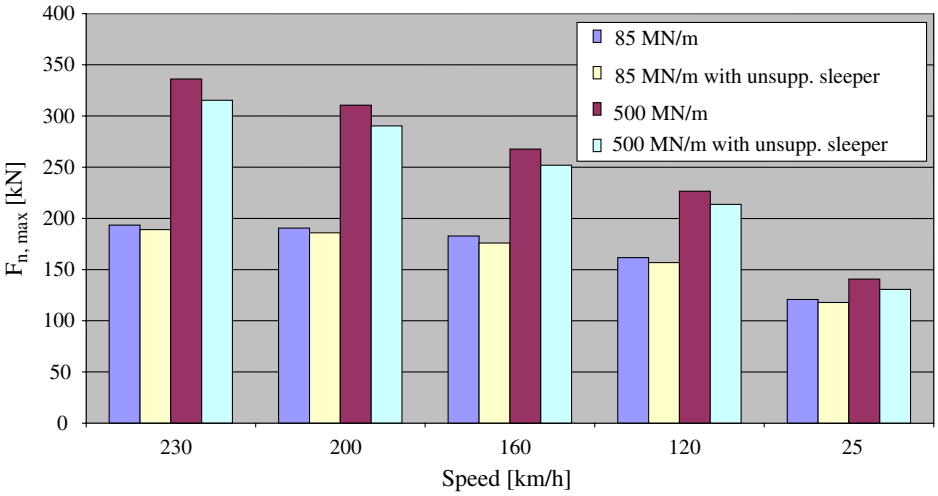

Fig. 13 Influence of train speed and track stiffness on the maximum normal contact force on Loco BR 101 ($Q_0 = 107$ kN), S1002, EH 60-500-1:12, facing move

of several parameters was investigated. The simulation results show that impact loads in the crossing panel increase with increasing speed and wheel load, see Fig. 13. The vertical track stiffness in the crossing panel is also investigated. The results of the investigation are illustrated in Fig. 13. An interesting result is that a reduction of track stiffness from 500 to 85 MN/m, due to the use of elastic rail pads, leads to significantly lower normal contact forces and an increasing effect with increasing speed. Also in the case of one unsupported sleeper below the transition area of the crossing, slightly reduced impact loads can be observed. Thus, the modification of track stiffness in the crossing panel indicates a high potential for the reduction of material degradation of a crossing nose.

4 SIMULATION OF MATERIAL DEGRADATION IN SWITCHES AND CROSSINGS

To predict the overall degradation of S&C components, it is necessary to consider the three damage mechanisms: plastic deformation, RCF, and wear. A methodology for simulating (predicting) all these mechanisms for a mixed traffic situation in an S&C has been developed [**3**]. The methodology is presented and demonstrated below.

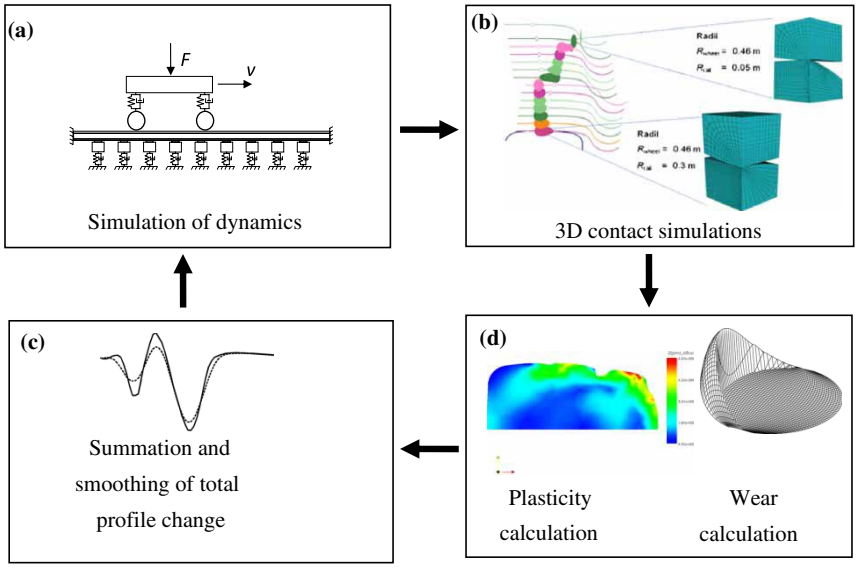

Fig. 14 Methodology for simulation of wheel–rail contact and damage in S&C: (a) simulation of dynamic wheel–rail contact forces; (b) calculation of contact stresses, contact patch sizes, and contact pressure; (c) simulation of plastic deformation and wear; and (d) summation and smoothing of profile change. From reference [**2**]

4.1 Simulation methodology

The methodology for predicting damage of S&C components involves an integration of several cross-disciplinary numerical tools (see Fig. 14). For a given S&C design (curve radius, crossing angle, steel grade, etc.) with a nominal (or initial) set of rail profiles, the methodology includes the following four steps, see also references [**2**] and [**3**].

1. Vehicle dynamics simulations to calculate wheel–rail contact forces, creepages, and contact positions. The influence of stochastic variations in vehicle loads (due to wheel profile, vehicle type, vehicle speed, and wheel position at switch entry) is considered by repeating the dynamic simulation with different sets of vehicle input data.
2. Wheel–rail contact simulations for each load cycle to determine non-Hertzian wheel–rail contact patches, taking into account the elasto-plastic material behaviour. The modelling of non-linear material behaviour is particularly important for S&C applications, where the contact pressures may be high due to severe dynamic loads and/or small contact patches. For each contact position, the outputs to the next step of the methodology are the contact patch size, the maximum von Mises equivalent stress, and the maximum contact pressure.
   (a) Finite element simulations for a large number of load cycles to predict the irreversible plastic deformations and work hardening of the material [**6**] at rail cross-sections with severe contact loads. The adopted rail material model is based on a formulation for hyperelastoplasticity that has been calibrated using cyclic uniaxial loading tests. Results from the contact simulations (step 2) and the slip, contact positions, and contact forces determined by the simulations of vehicle dynamics (step 1) are used as input.
   (b) Wear simulations at rail cross-sections with severe contact loads using FASTSIM [**7**] and the Archard wear model [**8**]. On the basis of FASTSIM, the contact patch is discretized into a grid.
3. Updating of rail profiles. The predicted profile of each studied rail cross-section after the load cycles have been applied is obtained by adding the calculated profile changes due to plastic deformation and wear. A smoothing process is then conducted on the basis of calculations of a moving average for each of these coordinates.

The new set of rail profiles are then used in simulations of vehicle dynamics with the same sets of stochastic vehicle input data. By performing the different steps in an iteration scheme, the gradual development of damage in the S&C components can be simulated for a given number of load cycles. The simulation methodology is described in more detail in reference [**3**].

To obtain accurate predictions of wheel–rail contact stresses (step 2) and plastic strains (step 3(a)) in S&C components, a calibrated material model of the rail steel is required. The adopted rail material model is presented in detail in reference [**6**]. In general, it is difficult or even impossible to perform laboratory tests where the specimens are subjected to similar loading situations as for an in-field S&C component. Owing to this difficulty, the calibrations of the material model have in this project been based on results from cyclic stress-controlled experiments on uniaxial tensile bars.

4.2 Simulation results and comparisons with measurements

Two demonstration examples of the use of the simulation methodology for calculation of rail profile degradation are presented: the switch panel (material R260) of a turnout at Härad in Sweden [**3**] and the frog (crossing nose and wing rails, material R350HT) of a turnout at Haste in Germany [**2**].

The Härad turnout is a standard (right turn) design UIC60-760-1:15 (with curve radius 760 m and turnout angle 1:15). The nominal variation of the rail profile (at 40 positions) in the switch panel was measured by MiniProf, with sampling distance in the order of 30 cm [**4**]. The multi-body dynamics code GENSYS is used to simulate vehicle motion, contact positions, contact patch sizes, and magnitudes of normal and tangential forces in the wheel–rail contacts. The freight vehicle model included two Y25 bogies. The track model is based on a co-following mass–spring–damper system that is coupled to each wheelset in the vehicle model (moving track model).

To improve the representation of the variation in wheel–rail contact load conditions that the switch rail is subjected to, wheel profile, train speed, and wheel–rail friction were taken as stochastic input parameters. The objective was to obtain a more realistic set of load cycles leading to a distribution of wear and plastic deformation over the width and along the switch rail. A representative traffic situation was given as input with Gaussian (normal) probability distributions for train speed v and friction coefficient μ. This together with 18 different wheel profiles (equal probability) gave, using Latin Hypercube sampling, a total of 92 load cases in a representative load sequence. Two different axle loads, 25 and 30 tonnes were compared.

The vertical contact force Q and the wear index parameters from the vehicle dynamics simulations were considered to identify the critical rail cross-sections in the switch panel. On the basis of these results, two critical rail cross-sections were identified: rail section 24 with the highest wear index and rail section 36 with the highest vertical contact force. For rail section 24, wear and plastic deformation gave

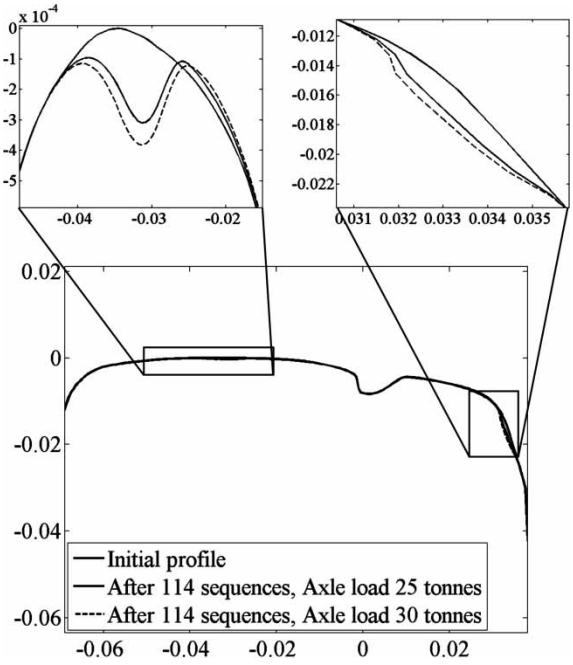

Fig. 15 Degradation of rail section 24 after 114 load sequences (about 10 000 load cycles) due to wear and plastic deformation. Rail material R260. Two different axle loads. From reference [**3**]

similar amounts of cross-section degradation after 114 load sequences (corresponding to about 10 000 load cycles). However, for rail section 36 the plastic deformation was the dominating damage mechanism. Increasing the axle load from 25 to 30 tonnes resulted in an increase of the vertical profile change by 27 per cent (see Fig. 15), whereas the numerical value of the RCF criterion was increased by 10 per cent for rail section 24.

The turnout at Haste was studied in a second demonstration example. It is a standard S&C design EH 60-500-1:12 subjected to traffic in the facing move. The dynamics was simulated in the multi-body dynamics code SIMPACK. The complete 3D vehicle models of a Loco BR 101 and of an ICE-T coach (BR 411), representing two different static wheel loads (107 and 67 kN, respectively), were used. The elastic properties (flexible modes) of car body, bogie frames, and wheelset were neglected. The track model is based on an FEM of elastic rails and elastic sleepers [**2**].

A load sequence was designed using Latin Hypercube sampling, taking into account four vehicle input variables: wheel profile, lateral wheel position at crossing entry, vehicle speed, and vehicle type. Results from five iterations of the simulation methodology are presented. In each iteration, $N_1 = 100$ load sequences were accounted for. Each of the load sequences nominally included $N_2 = 400$ load cycles, and thus a total of 40 000 load cycles were included in each iteration. However, in practice, some load cycles were excluded; e.g. load cycles where the wheel–rail contact conditions resulted in very small contact radii were neglected to avoid 3D contact simulations in step 2 of the methodology with poor finite element (FE)-mesh quality. The selected number of load sequences (in each iteration) was partly based on the aim, in a reasonable amount of computing time, to account for a number of load cycles that were comparable to the traffic load during the field tests in Haste. After the five iterations, the crossing model had been subjected to a total of $N_3 = 500$ load sequences corresponding to in the order of 200 000 load cycles. These 200 000 load cycles correspond to roughly 5 weeks of traffic in Haste.

Results from MiniProf measurements of the crossing nose on three different occasions are presented in

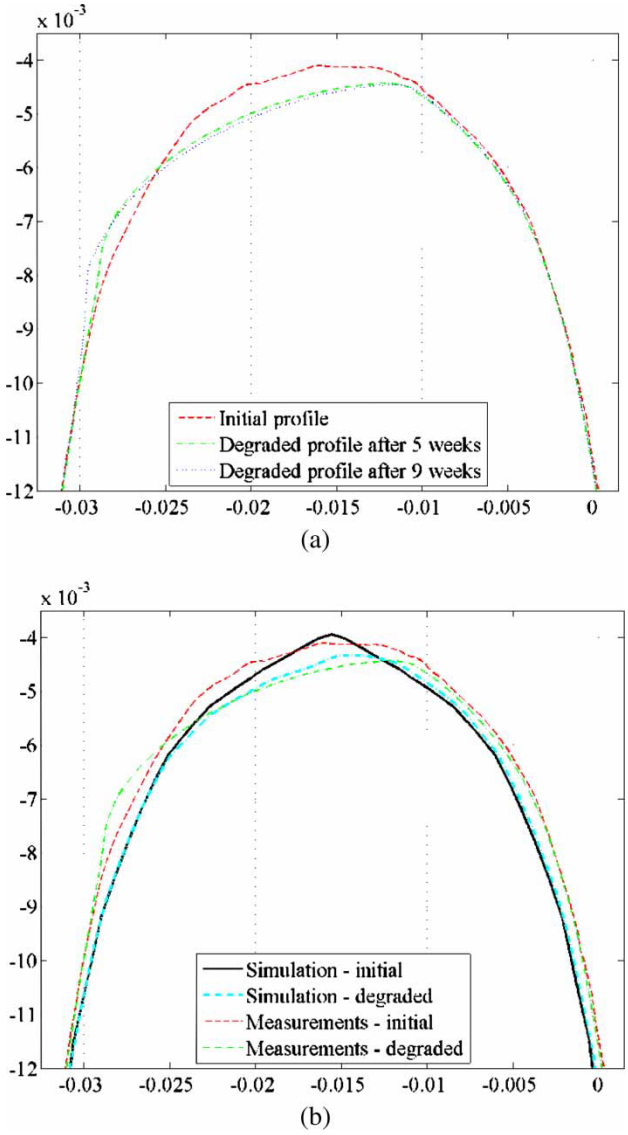

Fig. 16 (a) Crossing nose profile on the basis of measurements in Haste and (b) comparison between measurements (5 weeks) and numerical simulation (500 sequences). Rail material R350HT. Dimensions in metres. From reference [**2**]

Fig. 16(a). The measurements of the degraded profile were performed after 5 and 9 weeks of installation. It is seen that the degradation rate is larger during the first weeks after installation and then it seems to stabilize. The rail profile change of the crossing nose and wing rails made of R350HT steel was simulated for nine cross-sections. Good qualitative agreement was observed between the simulated and the measured rail profile change after 5 weeks of mixed traffic, see Fig. 16(b). More specifically, the largest degradations were found for similar longitudinal positions along the crossing nose (approximately 300 mm away from the tip of the crossing nose), and the simulated and measured profile changes were found to be of the same order of magnitude (approximately 0.5 mm). Plastic deformation was observed to be the dominating degradation mechanism in the beginning, whereas wear dominated in the end of the degradation process.

5 CONCLUSIONS

The numerical simulations presented here show that the switch panel design can be improved by applying a dynamic gauge widening (gauge optimization) at the switch entry. The gauge optimization process was based on varying a single parameter (maximum gauge widening), which represented the gauge optimization geometry. For traffic in the facing and trailing moves of the through route, an optimum solution was identified and then evaluated by a wider set of simulation cases (using different wheel profiles). The optimum design includes a 12 mm maximum gauge widening. The main benefits obtained by the proposed design are a significant reduction of wear along the switch panel and a significant reduction of the RCF index, and therefore improved behaviour in terms of RCF. In addition, the proposed geometry modification with a widening of the gauge at switch entry could relieve the flange contact with the switch rail at the early stage by steering the wheel towards the other rail. Furthermore, with this geometry modification, the tip of the switch rail could be thicker, which gives more material to resist wear and hence reduces the life-cycle cost (LCC) for the switch. The optimized geometry showed more consistency in the results (a significant reduction of wear and RCF indices compared to the nominal design) when using a range of wheel profiles.

For track stiffness optimization, two alternative stiffness variation models were considered. The influences on wear index and wheel–rail contact forces were investigated. The stiffness variation is expected to be achieved by varying the rail pad stiffness along the switch panel or by applying under sleeper pads. Placing stiffer rail pads starting from some distance before the front of the turnout and softer rail pads close to the switch heel can improve the smoothing of the large change in track stiffness along the switch panel. A considerable reduction in wear index is obtained (up to 80 per cent on the peak value) when varying the rail pad stiffness by a maximum of ± 30 per cent and ballast/subgrade stiffness values by a maximum of ± 20 per cent.

The numerical assessment of contact loads for a crossing panel with reduced support stiffness (by means of elastic rail pads), instead of the standard support stiffness, showed that impact loads can be reduced considerably, especially for crossing negotiation at high speed. Investigations of different crossing geometries showed that it is difficult to find a solution that leads to a force reduction for all wheel profiles occurring in service. Nevertheless, the MaKüDe crossing design showed the best performance for moderately worn wheel profiles in both running directions (facing and trailing moves). In combination with a reduced support stiffness, this crossing design will lead to a significant reduction in the impact loads and consequently has a high potential for LCC reduction.

A methodology for simulating (predicting) rail profile deterioration due to wear, accumulated plastic deformation, and RCF for a mixed traffic situation in an S&C has been developed. The methodology includes simulation of dynamic vehicle–track interaction considering stochastic variations in input data, simulation of wheel–rail contacts accounting for nonlinear material properties and plasticity, and simulation of wear and plastic deformation in the rail during the life of the S&C component. Two examples demonstrating the use of the simulation methodology were reported. In the first example, the influence of increased axle load on the degradation of a switch panel (switch rail and stock rail) was studied. In the second example, rail profile degradation at the frog (crossing nose and wing rails) of a turnout at Haste in Germany was investigated. For the latter example, simulation results were compared with measurements after 5 weeks of mixed traffic. Good qualitative agreement was found for the damage to the crossing nose, which validates the simulation methodology. A number of possible parameter investigations can now be performed with the proposed simulation methodology to study the influence of, for example, traffic situation (vehicle type, speed, axle load, etc.), switch geometry, and material of switch components.

ACKNOWLEDGEMENTS

The authors wish to acknowledge the support of the European Commission under the FP6 'INNOTRACK' project.

REFERENCES

1 **Kassa, E., Iwnicki, S., Perez, J., Allen, P.,** and **Bezin, Y.** Optimisation of track gauge and track stiffness along a switch using a multibody simulation tool. In Proceedings of the 21st International Symposium on *Dynamics of vehicles on roads and tracks*, Stockholm, Sweden, 17–21 August 2009 (available on CD).

2 **Nicklisch, D., Nielsen, J. C. O., Ekh, M., Johansson, A., Pålsson, B., Zoll, A.,** and **Reinecke, J. M.** Simulation of wheel–rail contact and subsequent material degradation in switches & crossings. In Proceedings of the 21st International Symposium on *Dynamics of vehicles on roads and tracks*, Stockholm, Sweden, 17–21 August 2009 (available on CD).

3 **Johansson, A., Pålsson, B., Ekh, M., Nielsen, J. C. O., Ander, M. K. A., Brouzoulis, J.,** and **Kassa, E.** Simulation of wheel–rail contact and damage in switches & crossings. In Proceedings of the 8th International Conference on *Contact mechanics and wear of rail/wheel systems*, Florence, Italy, 15–18 September 2009, pp. 987–996.

4 **Kassa, E.** and **Nielsen, J. C. O.** Dynamic interaction between train and railway turnout: full-scale field test and validation of simulation models. *Veh. Syst. Dyn.*, 2008, **46**(1), 521–534.

5 **Ekberg, A., Kabo, E.,** and **Andersson, H.** An engineering model for prediction of rolling contact fatigue of railway wheels. *Fatigue Fract. Eng. Mater. Struct.*, 2002, **25**(10), 899–909.

6 **Johansson, G., Ahlström, J.,** and **Ekh, M.** Parameter identification and modeling of large ratcheting strains in carbon steel. *Comput. Struct.*, 2006, **84**(15–16), 1002–1011.

7 **Kalker, J. J.** A fast algorithm for the simplified theory of rolling contact. *Veh. Syst. Dyn.*, 1982, **11**(1), 1–13.

8 **Archard, J. F.** Contact and rubbing of flat surfaces. *J. Appl. Phys.*, 1953, **24**, 981–988.

APPENDIX

Notation

a	semiaxis of the Hertzian contact patch
b	semiaxis of the Hertzian contact patch
d	maximum gauge widening
F_{n}	normal contact force
FI_{surf}	surface-initiated RCF index
k	yield limit in pure shear
k_{b}	combined sleeper and ballast stiffness (the structure underneath the rail pad)
k_{p}	combined rail and rail pad stiffness
L_{Jump}	length from the beginning of the turnout to the contact point jump location
L_1	length for which the curvature in the dynamic gauge variation is R_{C}
L_{Total}	total length of the dynamic gauge variation from the beginning of the turnout
N_1	number of load sequences for one iteration
N_2	number of load cycles
N_3	number of load sequences for five iterations
Q	vertical contact force
Q_0	static wheel load
R_{C}	curvature of the diverging route
R_{Out}	curvature of the stock rail after the jump point has passed
T_x	creep force in the longitudinal direction
T_y	creep force in the lateral direction
$T\gamma$	wear index
γ_x	creepage in the longitudinal direction
γ_y	creepage in the lateral direction
μ	friction coefficient
v	train speed
$\sigma_{\mathrm{e,max}}$	maximum von Mises equivalent stresses